Performances of holographic gratings monitored by laser-induced phase separation in liquid mixtures

Stéphanie Buil,* Emmanuel Hugonnot, and Jean-Pierre Delville†
Centre de Physique Moléculaire Optique et Hertzienne, UMR CNRS/Université No. 5798, Université Bordeaux I, 351 Cours de la Libération, F-33405 Talence cedex, France
(Received 2 October 2000; published 26 March 2001)

We theoretically describe and experimentally explore the kinetics of holographic grating formation resulting from different laser-induced phase separation mechanisms. Our method makes use of two interfering c.w. laser waves to quench binary mixtures in composition, and to optically trap the nucleated domains on the fringes. Essentially, two different processes can lead to these variations in concentration: electrostriction and thermodiffusion. The former originates from induced dipolar couplings in a field gradient; as photopolymerization, this is a local process which is essentially sensitive to the $q=q_0$ Fourier mode forced by the fringe modulation. The latter corresponds to a variation in composition driven by a small thermal gradient; as solvent evaporation and thermal heating techniques, it is nonlocal and behaves as $1/q^2$ because of its dissipative origin. By making experiments in both cases, we show that this q dependence on excitation has a strong influence on the performance of holographic gratings. While in the first case reflectivity saturates because the phase transition is confined by the fringes which behave as separated optical boxes with ''soft walls'' which calibrate the droplet size, blurring is expected for fringe-trapped domains induced by a nonlocal phase transition because the transition is governed by the Gaussian shape of the pump beams, and nucleated domains can reach a much larger size than the fringe spacing. The good agreement observed with our general model clearly illustrates how to make the difference between local and nonlocal excitations, and offers a first step towards a unified description of holographic grating formation monitored by phase transitions.

DOI: 10.1103/PhysRevE.63.041504 PACS number(s): 64.70.Ja, 42.40.Pa, 82.70.Kj

I. INTRODUCTION

Organization of matter on a microscopic scale is of crucial interest for successful developments in holographic data storage and diffractive optics [1]. If surface relief modulation effects are widely used in applications [2], an attractive alternative is the emergence of bulk composite materials, because they exhibit many advantages such as combination of high diffraction efficiencies with both narrow band wavelength and angle selectivity [3]. Among the variety of artificial media used for such holograms (photopolymers [4], photorefractive crystals [5], ...), those resulting from a phase transition are very appealing. Indeed, by quenching a liquid mixture inside the miscibility gap, the system becomes intrinsically inhomogeneous due to nucleation and growth of droplets constituted by the minority phase in coexistence. Polymer-dispersed-liquid crystals (PDLC) [6], i.e., materials composed of liquid crystal-rich droplets dispersed in a polymer-rich matrix, are maybe the most well-known illustration of such composites. The droplets are usually formed via (i) temperature-induced [7], (ii) solvent evaporation-induced [8], or (iii) polymerization-induced [9] phase separation. In the first case, a homogeneous mixture of polymer and liquid crystal is prepared and the temperature is changed so that the two components are no longer miscible. On the other hand, even if solvent evaporation is usually monitored by temperature variations, now the transition is not directly thermally-driven but results, in fact, from a quenching in composition induced by an increase in solute concentration (here the liquid crystal). Finally, in polymerization-induced phase transition, the initial mixture is composed of monomers and liquid crystal, and the separation is generated by polymerizing the monomers.

Although the basic principles of operation are rather simple, any particular application requires a carefully controlled and tailored adjustment of the properties of the material. Understanding the droplet growth and droplet pattern organization is then crucial because the performances of the final devices depend on the size, shape, and distribution of these droplets. Due to the number of nonequilibrium processes involved, the coupling between phase separation and ordering makes this problem in morphogenesis rich and challenging. It also implies that control of these processes is a difficult task, not only because the droplet growth needs to be tailored but also because metastability is a key phenomenon of first-order phase transitions. Indeed, nucleation is known to occur spatially at random and to be initiated irreversibly by bursts due to the high sensitivity of the nucleation rate to even small thermodynamic fluctuations [10]. Moreover, the intrinsic polydispersity of the droplet distribution usually strongly decreases the signal/noise ratio of the expected response of the induced heterogeneous material [11].

There have been striking advances towards a better control of the material heterogeneity when Sutherland *et al.* [12] implemented a single step process in which the laser field distribution simultaneously induces the transition and orga-

*Electronic address: stephanie.buil@physique.uvsq.fr
†Electronic address: delville@cribx1.u-bordeaux.fr

nizes the droplet patterning. In their experiment, a prepolymer syrup consisting of a mixture of liquid crystal, monomers, and photoinitiator was irradiated by two interfering pump beams. Liquid crystals droplets were formed within the polymerized sample in a similar spatially periodic pattern with a size that seemed to be monitored by the fringe spacing. While this experiment is a beautiful illustration of a local coupling (i.e., in direct correspondence to the field distribution), in both thermal and evaporation methods this locality is lost because the origin of the quenching becomes dissipative; it is indirectly driven by the field through the heat deposited by the wave in the medium. However, understanding of these various phenomena is still at an early stage [13] because their theoretical description involves subtle couplings between diffusion-driven kinetics effects (phase transition, phase separation) and properly fashioned inhomogeneous electromagnetic field.

The present study is devoted to the analysis of these couplings. We theoretically describe and experimentally explore the kinetics of holographic grating formation resulting from laser-induced phase separation. Experiments are realized in a classical binary liquid mixture with a composition close to a liquid–liquid critical point. Even if the structure of such a medium is more simple than that of mixtures usually considered in holographic recording (polymer/liquid crystal mixture, for instance), our choice was motivated by the hope of providing a simple and universal description of the involved processes. Indeed, to fully understand the grating formation, a thermodynamic description of the kinetics of the induced transition is required. Such a theory exists for simple binary mixtures [14], which generally belong to the universality class ($d=3$, $n=1$) of the Ising model; d is the space dimension and n that of the order parameter, here the concentration. Moreover, from the experimental point of view, the use of quasicritical fluids is particularly interesting because (i) close to a critical point laser couplings are generally huge and easy to observe [15]; and (ii) due to universality, results obtained for a particular mixture are totally transportable to any mixture belonging to the same Ising class. Our method uses interfering c.w. laser waves to quench binary liquid mixtures in temperature and composition, and to optically trap the nucleated domains in the high intensity regions [16]. Essentially, two different processes can lead to these variations in composition: electrostriction [17] and thermodiffusion [18]. The former results from the coupling of the induced dipole moment generated by the field on each particle of solute with the gradient of this field. As for photopolymerization, this is a local process. The latter takes into account indirect thermal effect. Even off-resonance, a wave is usually slightly absorbed in the mixture due to a residual absorption of the components. The resulting weak beam-centered temperature gradient can give rise to a small thermal contribution of the optical quench for low critical point mixtures [19]. For our mixtures, this contribution is negligible. However, despite its weakness, the overheating can induce large concentration gradients via a thermodiffusive process, particularly in the vicinity of a liquid–liquid critical point where the Soret constant presents a diverging behavior. On contrary to dipolar couplings, thermodiffusion is nonlocal in nature. As for the solvent evaporation technique, thermodiffusive concentration variations do not follow exactly the electromagnetic field distribution because they are induced by a heat flow, resulting here from light absorption.

By making the experiment with two interfering beams, the phase separation is driven by the fringe pattern and confined in the excited bulk area; rigid boundaries play no role. Moreover, if the nucleated droplets are also optically trapped by the field gradient of these fringes, a droplet grating is generated, whose properties and patterning will depend on the excitation process. As a consequence, by making experiments in simple binary fluids, it is easy to mimic observations made in much more complicated mixtures, with the advantage that a full theoretical description can be implemented and compared to experimental results. This was our main motivation in investigating the dynamics of holographic grating formation resulting from a first order phase transition.

This paper is organized as follows. In Sec. II, we present the fundamental processes involved during an optical quench in composition driven by two interfering pump beams in a binary liquid mixture. We also describe the growth of the droplets nucleated by the field in a fringe pattern and deduce the dynamic reflectivity of the resulting droplet grating. Since behaviors depend on the excitation process, the comparison between local and nonlocal couplings is particularly developed. The mixtures used to experimentally illustrate the expected droplet grating reflectivities are described in Sec. III. Without loss of generality, we choose near-critical micellar phases of microemulsions as test media to give an universal description (associated to criticality) and to improve the comparison with models (the mesoscopic nature of these suspensions strongly increases signal/noise ratio in experiments). Section IV is devoted to the experimental setup. Experimental results for both local and nonlocal couplings are then presented and discussed in Sec. V. We finally conclude in Sec. VI with the opportunity offered by this work to open a general discussion on holographic gratings monitored by laser-induced phase transitions.

II. ELECTROSTRICTIVE VERSUS THERMODIFFUSIVE PHASE SEPARATION INDUCED BY TWO INTERFERING BEAMS IN BINARY LIQUID MIXTURES

A. Governing equations for the induced transition

Let us consider a binary liquid mixture far from the liquid-gas transition. Then, its thermodynamic properties can be described by the temperature T, the volume concentration in solute Φ, and the hydrostatic pressure. However, for mixtures close to a liquid–liquid transition submitted to a low power c.w. laser radiation, global density fluctuations resulting from a field-induced hydrostatic compression are negligible compared to the field variations of concentration driven by osmotic compressibility. Then, we suppose in the following that the hydrostatic pressure remains constant, even during the application of a laser wave. Let Φ_0 and T_0 denote the values of Φ and T in the absence of electromagnetic wave and Φ_E and T_E their field variations. Φ_E and T_E can easily be evaluated at the first order, with respect to the in-

tensity distribution $I(\vec{r})$, by solving the field-modified heat and mass transfer equations [20]. Since the thermal diffusivity χ_T is much larger than the solute diffusion constant $D^- = K_B T_0/6\pi\eta\xi^-$, where ξ^- is the correlation length of density fluctuations inside the coexistence curve and η is the bulk viscosity, the small overheating can be assumed as almost instantaneous compared to the nucleation time scale. Then, these equations become

$$\frac{\partial \Phi_E}{\partial t} = D^- \left[\vec{\nabla}^2 \Phi_E + \frac{\varrho_0}{\varrho_s} \frac{k_T}{T_0} \vec{\nabla}^2 T_E(\vec{r}) - \frac{\varepsilon_0 K_T \Phi_0^2}{2} \left(\frac{\partial \varepsilon_M}{\partial \Phi} \right)_T \vec{\nabla}^2 |\vec{E}|^2(\vec{r}) \right], \tag{1a}$$

$$\Lambda_{\text{th}} \vec{\nabla}^2 T_E(\vec{r}) + \alpha_a I(\vec{r}) = 0, \tag{1b}$$

where ϱ_0, ϱ_s, α_a, and Λ_{th} are respectively the initial density, the solute density, the absorption coefficient at the wavelength used, and the thermal conductivity. $I(\vec{r}) = 1/2\varepsilon_0 \sqrt{\varepsilon_M} c |\vec{E}|^2(\vec{r})$ is the field intensity, where c is the light velocity in vacuum, ε_M and ε_0 correspond respectively to the dielectric constant of the medium and to the dielectric permittivity, and $\vec{E}(\vec{r})$ represents the slowly varying amplitude of the optical field (i.e., its mean value over one optical period). The second and the third terms of the rhs of Eq. 1(a) describe, respectively, the thermodiffusive variation of concentration driven by the wave-induced thermal gradients and the osmotic compression of the solute resulting from electrostrictive forces generated by field gradients. Thermodiffusion is characterized by the Soret constant k_T while electrostriction is proportional to the osmotic compressibility K_T.

For a Fourier component $I(q)$ of the intensity distribution, where $q \neq 0$ is the modulus of an excited spatial wave vector $\vec{q}$, the time dependence of the field-induced variation in composition is given by [21]

$$\Phi_E(q,t) = \Phi_E(q,t=\infty)[1 - \exp(-D^- q^2 t)]. \tag{2}$$

Equation (2) shows that $\tau_D = 1/D^- q^2$ represents the characteristic time scale of a quench in composition. $\Phi_E(q,t=\infty) = \Phi_{\text{el}}(q,t=\infty) + \Phi_{\text{th}}(q,t=\infty)$ is the sum of the steady-state electrostrictive and thermodiffusive Fourier contributions, respectively given by

$$\Phi_{\text{el}}(q,t=\infty) = \frac{\varepsilon_0 K_T \Phi_0^2}{2} \left(\frac{\partial \varepsilon_M}{\partial \Phi} \right)_T |\vec{E}|^2(q) \tag{3}$$

and

$$\Phi_{\text{th}}(q,t=\infty) = -\frac{\varrho_0}{\varrho_s} \frac{k_T}{T_0} T_E(q), \tag{4a}$$

with

$$T_E(q) = \frac{\alpha_a}{\Lambda_{\text{th}}} \frac{I(q)}{q^2}. \tag{4b}$$

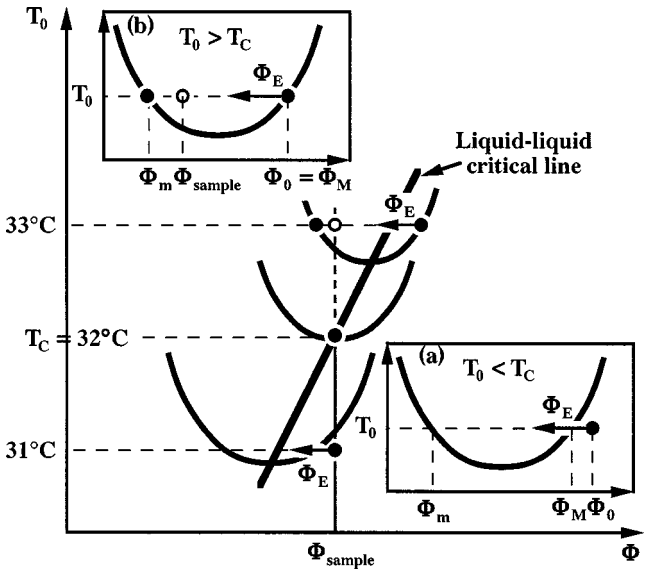

FIG. 1. Schematic phase diagram of our system as a function of temperature T_0 and volume concentration in solute Φ. Φ_{sample} corresponds to the chosen composition and T_C denotes the critical temperature; Φ_M and Φ_m are, respectively, the concentration of the majority and the minority phases in coexistence. Φ_E represents the quench in composition induced by the field distribution from the initial point (Φ_0, T_0). Insets: (a) situation for $T_0 < T_C$ $(\Phi_0 = \Phi_{\text{sample}})$; (b) situation for $T_0 > T_C$ $(\Phi_0 = \Phi_M)$.

Note that the nonlocality of thermodiffusion appears through the $1/q^2$ behavior of $T_E(q)$; since $\Phi_{\text{th}}(q,t=\infty)$ corresponds to the exact image of the temperature distribution, it is not only proportional to the local field intensity but also depends on the thermal boundary conditions in the medium.

These concentration variations can be used to quench a binary liquid located in composition in the vicinity of its coexistence curve and to analyze the decay of the resulting metastable state [16]. If $\Phi_E(q,t) < 0$, as in our experiments, the concentration in solute decreases in the high laser intensity regions. Thus, in the low critical point mixtures described below, the system can be quenched optically if Φ_0 is located in the high concentration side of the phase diagram close to the coexistence curve, as schematically illustrated in Fig. 1. Note the generality of the mechanism since the quenching procedure is symmetric for a mixture characterized by $\Phi_E(q,t) > 0$; Φ_0 has simply to be chosen close to the low concentration side of the coexistence curve. As a result, at some field-dependent nucleation time t_c which should be defined (see below), droplets constituted by the minority phase in coexistence Φ_m are nucleated by the field in the majority phase Φ_M.

To grow, the nucleated droplets must stay inside the fringe pattern. In fact, this condition is automatically satisfied for an electrostrictive quench. Let us assume $\Phi_{\text{el}}(q,t) < 0$, which corresponds to the situation depicted in Fig. 1. In this case, the volume concentration of solute Φ_m inside the nucleated domains is smaller than that of the surrounding phase Φ_M. But according to Eq. (3), $\Phi_{\text{el}}(q,t) < 0$ also means that $(\partial \varepsilon_M / \partial \Phi)_T < 0$. Thus the nucleated droplets necessarily have a refractive index larger than that of Φ_M. As a conse-

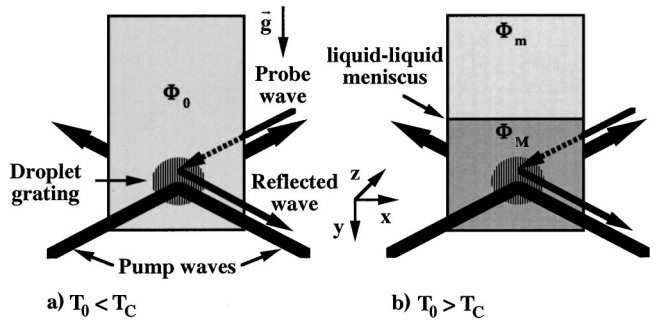

FIG. 2. Experimental configuration for $T_0<T_C$ and $T_0>T_C$. The grid mimics the grating induced in the phase Φ_M.

quence, their optical polarizability is positive, and they are optically trapped in the high field intensity regions. This automatic trapping condition is not surprising for electrostriction since the same dipolar mechanism is involved in the quench itself and in the optical trapping of the nucleated droplets [17]. For a quench in composition driven by thermodiffusion, the situation is not as clear because the sign of k_T depends on the properties of the entropy of mixing [18], which are not related to the refractive index contrast between Φ_m and Φ_M. Thus it is impossible to conclude in a general way about the optical trapping properties in this case. In the following, the mixture used for the analysis of thermodiffusion-induced phase transition will be then chosen so as to ensure the trapping of the nucleated domains in illuminated areas.

Finally, we must note that the first observable laser-driven effect is a small increase in temperature $T_E(q)$ associated to the low optical absorption at the wavelength used. It leads to a third contribution of the optical quench which, according to $\chi_T \gg D^-$, can be considered as almost instantaneous. Since waves are not resonant, this thermal component represents in our investigation a shallow effect which can be neglected compared to the concentration variation when analyzing the late stage kinetics of phase separation [22]. Due to its relevance in numerous applications, this coupling will be briefly discussed in Sec. II D.

To use these composition variations for building holographic gratings, we consider two linearly polarized c.w. TEM_{00} Gaussian waves of same intensity which interfere with an angle θ (Fig. 2). Thus, as shown in Fig. 3, three wave vector distributions of width $2/a_0$, where a_0 is the beam-waist of the pumps at beam intersection, are excited in the medium. If Λ_0 denotes the induced fringe spacing and $q_0 = |\vec{q}_0| = 2\pi/\Lambda_0$, these distributions are respectively centered around $\vec{q}=\vec{0}$, $\vec{q}=\vec{q}_0=\vec{k}_2-\vec{k}_1$ and $\vec{q}=-\vec{q}_0=\vec{k}_1-\vec{k}_2$ (where $\vec{k}_1$ and $\vec{k}_2$ are the wave vectors of the two pump beams). The distribution centered around $\vec{q}=\vec{0}$ (denoted in the following $\overline{q}=0$) represents the contribution of the Gaussian intensity shape of the pumps themselves while those centered around $\vec{q}_0$ and $-\vec{q}_0$ (denoted $q=q_0$ in the following) describe the modulation Λ_0 of the interference pattern.

Since concentration variations induced by a local coupling, here electrostriction, are directly proportional to intensity, the $\overline{q}=0$ and $q=q_0$ contributions have same amplitude

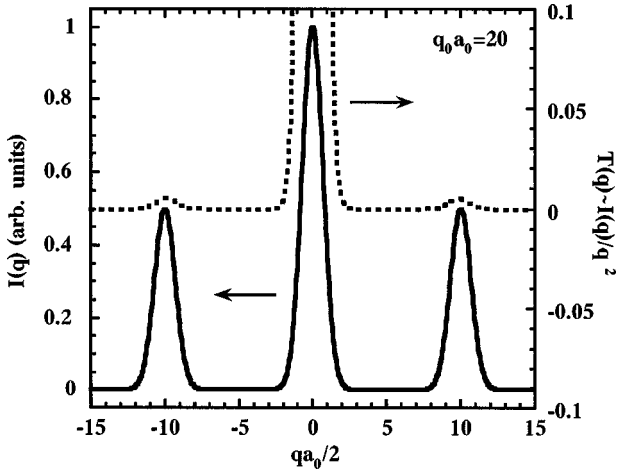

FIG. 3. Fourier representation of local ($\propto I(q)$) and nonlocal ($\propto I(q)/q^2$) excitations induced by two interfering TEM_{00} Gaussian pump waves for $q_0a_0=20$; a_0 and q_0 are, respectively, the beam-waist of the pump and the Fourier component associated with the fringe spacing.

in the medium (see Fig. 3). To increase the signal/noise ratio in experiments, we also choose $q_0a_0 \geqslant 10$. Then, the mass diffusion time scale associated to the $\overline{q}=0$ mode is at least one hundred time larger than that corresponding to the fringe spacing and we can consider that variations in composition are totally driven by the $q=q_0$ mode. As a consequence, a plane wave approximation can be used close to the beam crossing and the intensity distribution can be written as

$$I(x)=I_0[1+\cos(q_0x)], \tag{5}$$

where $I_0=(P/\pi a_0^2)$ and P is the total power injected into the sample. Using Eq. (3), the electrostrictive contribution at the center of the fringe pattern ($x \ll a_0$) becomes

$$\Phi_{\rm el}(x,t) \approx \Phi_{\rm el}^{q=q_0}(x,t) = 2\frac{K_T\Phi_0^2}{c}\left(\frac{\partial\sqrt{\varepsilon_M}}{\partial\Phi}\right)_T \frac{P}{\pi a_0^2} \times [1+\cos(q_0x)][1-\exp(-D^-q_0^2t)]. \tag{6}$$

This means that the phase transition driven by the field is almost completely monitored by the fringes; the Gaussian nature of the pumps is negligible.

On the other hand, Eqs. (4a)–(4b) shows that thermodiffusion is a nonlocal process because $\Phi_{\rm th}(q,t) \propto T_E(q) \propto I(q)/q^2$. Due to the $1/q^2$ behavior, the wave vector distribution centered around the $\vec{q}=\vec{0}$ mode is always strongly enhanced compared to any forced $\vec{q}=\vec{q}_0 \neq 0$ mode (see Fig. 3). This can also be illustrated in direct space by writing the inverse Fourier transform of $T_E(q)$ and $\Phi_{\rm th}(q,t)$ at beam intersection as $T_E(x)=T_E^{\overline{q}=0}(x)+T_E^{q=q_0}(x)$ and $\Phi_{\rm th}(x,t) = \Phi_{\rm th}^{\overline{q}=0}(x,t)+\Phi_{\rm th}^{q=q_0}(x,t)$. Using Eqs. (1a)–(1b), the pump beams contribution at the center of the fringe pattern is

$$T_E^{\overline{q}=0}(x) = \frac{\alpha_a P}{4\pi\Lambda_{\rm th}}\left[-E_1\left(\frac{x^2}{a_0^2}\right)-\ln\left(\frac{x^2}{a_{\rm cl}^2}\right)\right], \tag{7a}$$

$$\Phi_{\rm th}^{\bar{q}=0}(x,t) = -\frac{\varrho_0}{\varrho_d}\frac{k_T}{T_0}T_E^{\bar{q}=0}(x)\left[1-\exp\left(-\frac{D^-}{a_0^2}t\right)\right]. \tag{7b}$$

The distance $a_{\rm cl}(a_{\rm cl} \gg a_0)$ is defined by the thermal boundary condition $T_E^{\bar{q}=0}(x=a_{\rm cl})=0$ and $E_1(x)$ is the 1-argument Exponential Integral function. Besides, the fringe contribution to the concentration variation induced by thermodiffusion is

$$\Phi_{\rm th}^{q=q_0}(x,t) = -\frac{\varrho_0}{\varrho_d}\frac{k_T}{T_0}\frac{\alpha_a}{\Lambda_{\rm th}}\frac{1}{q_0^2}\frac{P}{\pi a_0^2} \times \cos(q_0 x)[1-\exp(-D^- q_0^2 t)t]. \tag{8}$$

Using $E_1(x \ll 1) \approx -\ln(\gamma x)+x$, where $\gamma = 1.781$ is the Euler constant, the ratio between those two contributions in the center of the central fringe is of the order of unity at short time $(t \ll 1/D^- q_0^2)$ and reaches $[\Phi_{\rm th}^{\bar{q}=0}/\Phi_{\rm th}^{q=q_0}](x=0,t=\infty) = (q_0 a_0/2)^2 \ln(\gamma a_{\rm cl}^2/a_0^2)$ at steady state. As a consequence, for $q_0 a_0 \geqslant 10$, the modulation of concentration induced by the fringe pattern becomes rapidly negligible compared to that generated by the Gaussian shape of the pump beams. A phase transition induced by thermodiffusion does not feel the existence of the fringe pattern. As illustrated in the following section, this difference in mode excitation between local and nonlocal couplings makes a huge modification in droplet growth and grating reflectivity, because the thermodynamic length scale switches from Λ_0 to a_0.

B. Droplet growth in a fringe pattern

To analyze the dynamic reflectivity of an induced droplet grating, it is necessary to build a model for the droplet growth in the fringe pattern. As already mentioned, for relatively unfocused waves, the symmetry of each pump beam is almost cylindrical around the propagation axis. However, despite this symmetry, the growing droplets are necessarily spherical due to a minimization of their surface energy. Unfortunately, a rigorous treatment of such symmetry mixing (growing spheres in a cylindrical quench), analogous to that encountered for droplet growth in a gravitational field [23], cannot be performed simply. Since our aim is to explore the general properties of holographic gratings built from laser-driven phase transitions and to obtain analytical results for easy interpretation of the experimental data, we will not take into account this geometric influence of surface tension. Instead, we will analyze the transverse growth of cylindrical droplets and assume that the predicted radius of the growing cylinders corresponds to that of the induced spherical droplets trapped by the fringes.

Unlike the spherical symmetry scenario where the single droplet problem may be solved directly from the steady-state equation for the solute diffusion, it is necessary here to consider an effective medium that will remove the unphysical singularity appearing in the concentration field; in cylindrical symmetry, the general solution of the stationary mass diffusion equation Eq. (1a) exhibits a logarithmic divergence at $r \to \infty$. Even if an *ad hoc* approach towards resolution is to introduce an arbitrary cutoff distance that prevents this divergence, it has been shown [24] that this method leads to incorrect results, even qualitatively. To solve the problem in a more appropriate way, Marqusee [24] considered an effective medium and derived self-consistently the growth rate of circular domains. We have extended Marqusee's model of two-dimensional Ostwald ripening to the laser-driven transverse growth of a beam-trapped cylindrical droplet of radius R and length l $(l \gg R)$. Let t_C denote the mean time needed to initiate nucleation in presence of the field. Then, in the adiabatic approximation [25], i.e., when the solute concentration around the growing droplets is almost stationary, the transverse three-dimensional diffusion-controlled growth rate of a cylindrical beam-trapped droplet nucleated by an optical quench in composition is [22]

$$\frac{dR}{dt} = \frac{D^-}{R}\left(\frac{R}{\zeta_E}\right)\frac{K_1(R/\zeta_E)}{K_0(R/\zeta_E)} \times \left\{ \frac{\Phi_E(R,t_C) + R\left(\frac{\zeta_E}{R}\right)\frac{K_0(R/\zeta_E)}{K_1(R/\zeta_E)}\left(\frac{\partial \Phi_E}{\partial r}\right)_{r=R,t=t_C}}{\Phi_m - \Phi_M} + \frac{\Phi_0 - \Phi_M}{\Phi_m - \Phi_M} - \frac{d_0}{R}\right\}, \tag{9}$$

where the screening length ζ_E satisfies the relationship:

$$(\zeta_E)^{-1} = 2\pi \int_0^\infty R[K_1(R/\zeta_E)/K_0(R/\zeta_E)]n(R,t)dR.$$

Here d_0 is a capillary length [26] and $K_0(x)$ and $K_1(x)$ are, respectively, the first and second modified Bessel functions. When comparing the experimental results with the model, we will assume that the variation of R/ζ_E, with the quench depth calculated numerically by Marqusee for the Ostwald ripening regime, still holds in the presence of the laser field. Equation (9) is very similar to the classical growth rate of a cylindrical domain for a spatially uniform quenching [24], except that now the supersaturation

$$\Phi_E(R,t_C) + R\left(\frac{\zeta_E}{R}\right)\frac{K_0(R/\zeta_E)}{K_1(R/\zeta_E)}\left(\frac{\partial \Phi_E}{\partial r}\right)_{r=R,t=t_C} + \Phi_0 - \Phi_M$$

becomes a function of both the field distribution and droplet radius. To illustrate the modification in behavior induced by the nonlocality or locality of the excitation, we particularize now Φ_E and separate the electrostrictive and the thermodiffusive processes, assuming that Φ_E is either $\Phi_{\rm el}$ or $\Phi_{\rm th}$.

1. Local growth rate in presence of electrostriction

As illustrated by Eq. (6) for a local process, the induced phase transition is monitored by the modulation of the interference pattern. Due to the finite extension of the fringe, they are independent from each other from the thermodynamic point of view, and the same growth law holds over all the fringes located at the center of the pattern, where the Gauss-

ian envelop of the pumps is negligible. We then consider the droplet growth inside the central fringe by assimilating its modulation to a transverse sine profile of extension Λ_0 with cylindrical symmetry. As a consequence, the droplet growth rate is simply described by Eq. (9), where Φ_E corresponds to $\Phi_{\mathrm{el}}(x,t_C)$ given by Eq. (6) which is rewritten as

$$\Phi_{\mathrm{el}}(x,t_C)=\frac{1}{2}(\Phi_{\mathrm{el}})_0[1+\cos(q_0 x)], \tag{10}$$

where

$$(\Phi_{\mathrm{el}})_0=\Phi_{\mathrm{el}}(x=0,t_C)$$

$$=4\frac{K_T\Phi_0^2}{c}\left(\frac{\partial\sqrt{\varepsilon_M}}{\partial\Phi}\right)_T\frac{P}{\pi a_0^2}[1-\exp(-D^- q_0^2 t_C)]$$

is the optical quench in composition on the axis of the interference pattern.

Without any alteration of generality, we assume $\Phi_0=\Phi_M$ for the description of the model. This means that the initial composition of the mixture is supposed to be located on its coexistence curve as for experiments presented in Sec. III [situation depicted in inset (b) of Fig. 1]. In this case, all the incident beam power is used for the quench. The droplet growth rate becomes:

$$\frac{dR}{dt}=\frac{D^-}{R}\left(\frac{R}{\zeta_E}\right)\frac{K_1(R/\zeta_E)}{K_0(R/\zeta_E)}\times\left\{\frac{1}{2}\frac{(\Phi_{\mathrm{el}})_0}{(\Phi_m-\Phi_M)}\left[1+\cos(q_0R)-\zeta_E\frac{K_0(R/\zeta_E)}{K_1(R/\zeta_E)}q_0\sin(q_0R)\right]-\frac{d_0}{R}\right\}. \tag{11}$$

2. Nonlocal growth rate in presence of thermodiffusion

As already shown, nonlocality in field variations in composition implies that the $q=0$ mode is always strongly enhanced compared to the intensity modulation of the interference pattern. For thermodiffusion, the quenching and the droplet growth are then essentially driven by the Gaussian shape of the pump beams despite the droplet trapping by the fringes. As a consequence, the droplet growth rate is simply described by Eq. (9), where Φ_E corresponds to $\Phi_{\mathrm{th}}^{\bar{q}=0}(x,t_C)$ given by Eq. (7b), which is rewritten as

$$\Phi_{\mathrm{th}}^{\bar{q}=0}(x,t_C)=(\Phi_{\mathrm{th}}^{\bar{q}=0})_0\frac{1}{\ln(\gamma(a_{\mathrm{cl}}/a_0)^2)}\times\left\{-E_1\left(\frac{x^2}{a_0^2}\right)-\ln\left(\frac{x^2}{a_{\mathrm{cl}}^2}\right)\right\}, \tag{12}$$

where

$$(\Phi_{\mathrm{th}}^{\bar{q}=0})_0=\Phi_{\mathrm{th}}^{\bar{q}=0}(x=0,t_C)$$

$$=-\frac{\varrho_0}{\varrho_S}\frac{k_T}{T_0}\frac{\alpha_a P}{4\pi\Lambda_{\mathrm{th}}}\ln\left(\gamma\frac{a_{\mathrm{cl}}^2}{a_0^2}\right)\left[1-\exp\left(-\frac{D^-}{a_0^2}t_C\right)\right]$$

is the optical quench in composition on the axis of the interference pattern. The droplet growth rate becomes

$$\frac{dR}{dt}=\frac{D^-}{R}\left(\frac{R}{\zeta_E}\right)\frac{K_1(R/\zeta_E)}{K_0(R/\zeta_E)}\times\left\{\frac{(\Phi_{\mathrm{th}}^{\bar{q}=0})_0}{(\Phi_m-\Phi_M)}\frac{1}{\ln(\gamma a_{\mathrm{cl}}^2/a_0^2)}\left[-E_1\left(\frac{R^2}{a_0^2}\right)-\ln\left(\frac{R^2}{a_{\mathrm{cl}}^2}\right)+2\left(\frac{\zeta_E}{R}\right)\frac{K_0(R/\zeta_E)}{K_1(R/\zeta_E)}\left(\exp\left(-\frac{R^2}{a_0^2}\right)-1\right)\right]-\frac{d_0}{R}\right\}. \tag{13}$$

3. Discussion in terms of locality

If $R\ll\Lambda_0/2$ (resp. $R\ll a_0$) for electrostriction (resp. thermodiffusion), Eqs. (11) and (13) reduce to the familiar expression of the droplet growth rate for spatially uniform quenches [26]:

$$\frac{dR}{dt}\approx\frac{D^-}{R}\left\{\frac{(\Phi_E)_0}{(\Phi_m-\Phi_M)}-\frac{d_0}{R}\right\}. \tag{14}$$

However, modifications appear at larger R. To show these differences, Fig. 4 illustrates the set of predicted radii in which $dR/dt=0$ versus the quench depth on the axis of the interference pattern. For a comparison, both electrostrictive and thermodiffusive couplings are depicted (assuming $(\Phi_{\mathrm{el}})_0=(\Phi_{\mathrm{th}}^{\bar{q}=0})_0$), as well as the classical behavior given by Eq. (14) which, as stated above, corresponds to small droplet radii. In the latter case, $dR/dt=0$ gives the set of critical radii R_C^E. This set is represented by a hyperbola, which simply means that the critical radius is inversely proportional to the quench depth; according to Eq. (14), $R_C^E=d_0/[(\Phi_E)_0/(\Phi_m-\Phi_M)]$. For an optical quench, the situation is more complicated. In the presence of waves, the stationary regime $dR/dt=0$ leads to a droplet radius that exhibits a cuvette shape as a function of the initial central quench depth. $dR/dt=0$ is positive inside this curve and negative outside. The left branch corresponds to the critical radius R_C^E variation while the right branch gives the maximum droplet radius R_{MAX}^E allowed by the finite size of the optical quench. This finite size effect also leads to a cutoff in the set of possible R_C^E; there is a maximum value of R_C^E which also represents the smallest accessible R_{MAX}^E. This is also associated with a minimum quench depth below which the transition cannot occur. This limitation shows that the beam size (resp. the fringe spacing) in thermodiffusion (resp. in electrostriction) reduces the set of accessible length scales for the droplet growth compared to a classical uniform quench.

Moreover, Fig. 4 also illustrates different behaviors, in terms of accessible droplet radii, for electrostrictive and thermodiffusive quenches in composition induced by the same

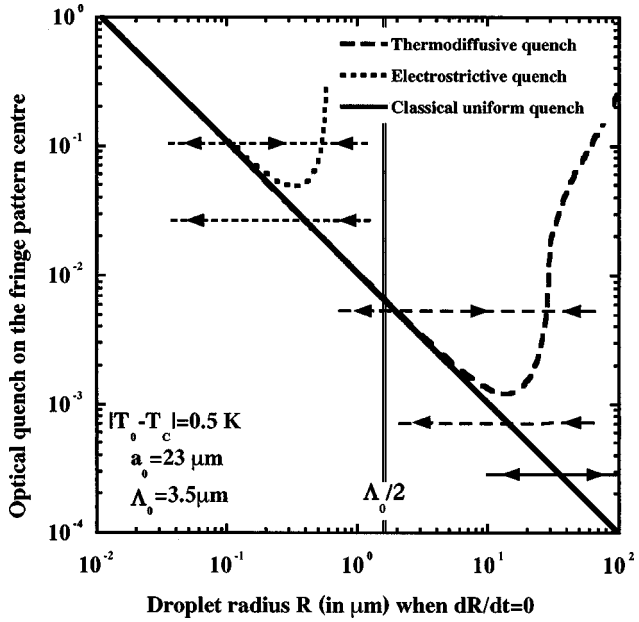

FIG. 4. Set of radii corresponding to a zeroth growth rate versus the optical quench depth at the center of the fringe pattern for both electrostrictive and thermodiffusive processes. The left (respectively right) part illustrates the behavior of the critical radius R_C^E (respectively maximum radius R_{MAX}^E) allowed by the different length scales of the intensity distribution; electrostriction is sensitive to the fringe spacing while thermodiffusion is monitored by the beam waist of the pumps. For a comparison, the variation for a classical uniform quench inside an infinite medium is also plotted. The arrows indicate the evolution of the droplet radius in the different regions separated by $dR/dt=0$.

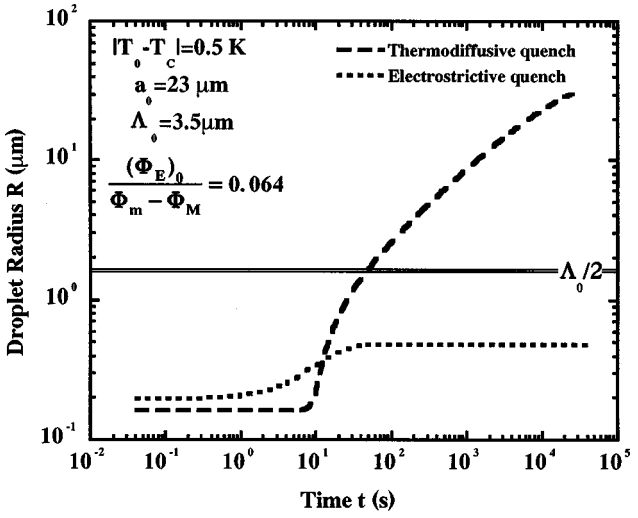

FIG. 5. Predicted droplet growth for a typical experimental quench depth (see experimental section) sufficient to drive a phase transition in both electrostrictive and thermodiffusive cases. The fringe spacing induces finite size effects on the electrostrictive growth while thermodiffusion is totally monitored by the extension of the pumps and does not feel the fringe pattern.

interfering pump beams. As discussed above, this difference is due to the local or nonlocal character of the quench. Since electrostriction varies linearly with field intensity, it is monitored by the fringe spacing, and droplet radii cannot be larger than $\Lambda_0/2$. On the contrary, for thermodiffusion, which is driven by the temperature dissipated in the medium, such a strong dependence does not exist and values of R_{MAX}^E even larger than the beam radii of the pumps are allowed [22].

To illustrate the saturation of the droplet radius towards R_{MAX}^E, and thus the appearance of a saturation regime at the late stage of the transition, we can compute the droplet growth behavior from Eqs. (11) and (13). Figure 5 illustrates the predicted variation for both couplings. Integration was done considering the initial condition $R(\tau_C^E=(R_C^E)^3/D^-\xi^-)=R_C^E+\xi^-/2$, where τ_C^E is the relaxation time associated with the critical radius R_C^E at the beginning of the quench and $\xi^-/2$ corresponds to an uncertainty on the activation barrier of nucleation of the order of k_BT [26]; note that $t_C=\tau_C^E$ when nucleation is homogeneous [26], i.e., when driven by the correlation length of density fluctuations.

Those curves are very important from the experimental point of view. Indeed, by definition, the reflectivity of an induced grating disappears as soon as $R(t)\geqslant\Lambda_0/2$. Then, as already mentioned in experimental investigations using thermal quenching [8], to obtain a good signal/noise ratio in presence of a nonlocal coupling, the experiment has to be stopped well before saturation of the droplet growth; remember that in this case the growth is essentially driven by the pump beams ($\overline{q}=0$ mode) instead of the fringe modulation. This procedure is always difficult to optimize because to many parameters can monitor a phase transition and transportation of an experimental scheme (calibration, etc.) from one sample to another is usually irrelevant. On the other hand, for a local coupling, such an external control is not necessary because the droplet growth is totally driven by the fringes. The growth increases progressively the grating reflectivity, which reaches a steady value at the end of the local phase transition when $R(t\rightarrow\infty)$ reaches the stable value R_{MAX}^E, tailored by the fringe spacing. The induced phase transition never blurs the grating reflectivity. Moreover, since droplets are self-calibrated by the fringes at the end of the local transition, the intrinsic droplet polydispersity appearing in classical phase transition totally disappears here. This aspect is very important for applications because it also increases the signal/noise ratio. These expectations are illustrated in the experimental section.

C. Reflectivity of a grating constituted by growing droplets

The reflectivity of the induced droplet grating (ratio of the diffracted to the incident probe beam intensities) is by definition [27]

$$\Re(z,t)=\frac{|\vec{E}_R(z,t)|^2}{|\vec{E}_P(z=0,t)|^2}. \tag{15}$$

The probe and the reflected waves, respectively $\vec{E}_P$ and $\vec{E}_R$, are determined using the nonlinear propagation equation in the medium

$$\vec{\nabla}^2\vec{E}-\frac{\varepsilon_M}{c^2}\frac{\partial^2\vec{E}}{\partial t^2}=\frac{1}{c^2}\frac{\partial^2}{\partial t^2}(\varepsilon_E\vec{E}), \tag{16}$$

where $\vec{E}$ represents the superposition of the four waves interacting in the medium (the two pump beams $\vec{E}_1$ and $\vec{E}_2$, $\vec{E}_P$ and $\vec{E}_R$) and ε_E corresponds to the modulation of the dielectric constant resulting from the induced droplet grating. By choosing $q_0a_0\geqslant 10$, Eq. (16) can be solved for planes waves in the slowly variable amplitude approximation; one finds for $\varepsilon_E\ll\varepsilon_M$ [15]:

$$\Re(z,t)=\left(\frac{2\pi z}{\sqrt{\varepsilon_M}\lambda_0}\right)^2[\varepsilon_E(t)]^2. \tag{17}$$

Equation (17) shows that the time dependence of the reflectivity is directly related to the modification of the dielectric constant induced by the field in the medium. This variation is generated by the increase in droplet volume concentration $\varphi_D^E(t)$ on the fringes resulting from the fringe trapping and the growth. Since in usual experiments nucleation is heterogeneous even in the bulk [28], i.e., nucleation is essentially driven by the unavoidable impurities present in the mixture, most of the droplets are nucleated on a finite number of seeds at the same mean nucleation time t_C. Thus $t_C<\tau_C^E$ and $\varphi_C^E(t\leqslant t_C)=0$. Moreover, for low quench depths, $\varphi_D^E(t)$ can be considered small enough to make a first-order development of the nonlinear dielectric constant modulation as

$$\varepsilon_E(t>t_C)\approx\left(\frac{\partial\varepsilon}{\partial\varphi_D}\right)_T\varphi_D^E(t). \tag{18}$$

The time dependent reflectivity becomes

$$\Re(z,t>t_C)=\left[\frac{2\pi z}{\sqrt{\varepsilon_M}\lambda_0}\left(\frac{\partial\varepsilon}{\partial\varphi_D}\right)_T\right]^2(\varphi_D^E(t))^2. \tag{19}$$

From the optical point of view, as soon as $t>t_C$, the medium can be assimilated to a dielectric assembly of very small droplets of volume concentration Φ_m suspended in a continuous phase of volume concentration Φ_M. For such a microscopic suspension, a continuous thermodynamic description has already been experimentally validated [29]. Thus $\varphi_D^E(t)$ can be described by a diffusion equation, analogous to Eq. (1a), in which the only field contribution is the electrostrictive manipulation of the nucleated droplets by the fringe pattern.

Then, if $[0,t_1]$ corresponds to the illumination time interval of both pump beams, the droplet grating formation for the excited Fourier component $q_0\neq 0$ is described by

$$\Re(t_C<t<t_1)\propto[\varphi_D^E(t)]^2, \tag{20a}$$

$$\frac{\partial\varphi_D^E}{\partial t}=-D_D(t)q_0^2[\varphi_D^E(t)+AR(t)^3], \tag{20b}$$

$$\frac{\partial R}{\partial t}\quad\text{given by Eq. (11) for electrostriction,}$$

$$\frac{\partial R}{\partial t}\quad\text{given by Eq.(14) for thermodiffusion,} \tag{20c}$$

where $D_D(t)=k_BT_0/6\pi\eta R(t)$ is the mass diffusion coefficient of a growing droplet of mean radius $R(t)$. $AR(t)^3$ is proportional to the droplet polarizability. To solve these equations, we use the following initial conditions: $\varphi_D^E(t=t_C)=0$ and $R_C(t=t_C)=R_C+\xi^-/2$. Finally, observation of a reflectivity induced by a droplet grating needs $R\leqslant\Lambda_0/2$. Then $R(t)\ll a_0$ for $q_0a_0\geqslant 10$, and the nonlocal growth rate reduces to the familiar behavior of an isolated droplet; finite size effects induced by the pumps are totally negligible at this stage and Eq. (13) reduces to Eq. (14).

Since for classical liquid mixtures the induced phase transition is reversible, i.e., initial homogeneous thermodynamic state is recovered when pumping is stopped, they are particularly suitable for a conceptual investigation of holographic grating generation. Indeed, we can easily increase the signal/noise ratio by accumulation. Even if such a property clearly needs to be avoided for practical applications, this reversibility is of particular importance towards a better understanding of the involved processes, because it increases the experimental value and allows a much better comparison between experiments and theory. So, let's assume that one pump beam is stopped by a chopper at $t=t_1$. As a consequence, optical fringes disappear and the grating relaxes. Moreover, a reverse quench [30], still within the two-phase region, is induced in the medium. Then, the growth momentarily slows down and we can assume that the droplet radius has not enough time to change noticeably during the grating relaxation. Since the droplet fringe trapping disappears, $\varphi_D^E(t>t_1)$ is simply described by

$$\frac{\partial\varphi_D^E}{\partial t}(t>t_1)=-D_D(t)q_0^2\varphi_D^E(t). \tag{21}$$

Therefore, during the grating relaxation the reflectivity behaves as

$$\Re(t>t_1)\propto\exp\left(-\frac{t-t_1}{\tau_R}\right), \tag{22}$$

where $\tau_R=1/2D_D(t=t_1)q_0^2\propto\Lambda_0^2R(t=t_1)$ is the characteristic relaxation time. As a consequence, the analysis of the reflectivity during the relaxation of the induced grating allows a direct measurement of the mean droplet radius at $t=t_1$ which can be compared independently to the growth law obtained from the grating formation. This two-step procedure is very powerful because one can continuously check the value of an experiment by the coherence between formation and relaxation of the induced grating. Before comparing these predicted behaviors with experimental observations, the next section briefly discusses the important case of a thermal quench driven by the wave. As already observed experimen-

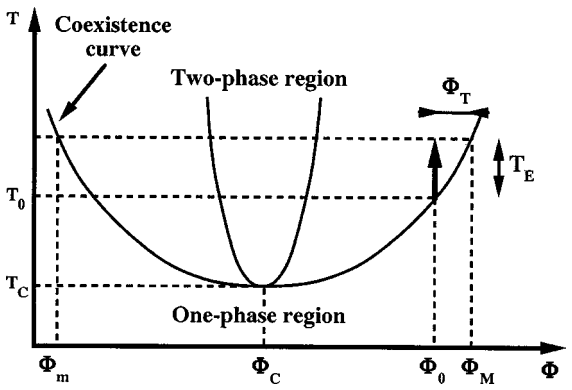

FIG. 6. Schematic phase diagram of a binary liquid mixture with an inverted coexistence curve. Φ is the volume concentration in solute and T is the temperature. Φ_C and T_C are the coordinates of the critical point and Φ_0 and T_0 characterize the medium before the application of a laser wave. Φ_T represents the supersaturation on the optical axis induced by a laser-driven thermal quench, T_E, resulting from the absorption of the wave by the medium. Φ_m and Φ_M are the coexisting compositions at temperature T_0+T_E.

tally [31], this process, weak in our mixtures, can dominate if the medium absorption at the wavelength used becomes large.

D. Nonlocal growth rate in presence of thermal quenching

As mentioned before, mixtures are often characterized by at least a small absorption of the wave at the used wavelength. We already show that the resulting nonlocal overheating is almost unaffected by the modulation of the fringe pattern: it corresponds to $T_E^{\bar{q}=0}$ given by Eq. (7a). As illustrated in Fig. 6, this field-variation of the temperature can also quench a liquid mixture if its phase diagram presents an inverted coexistence curve with a low critical point. To use all the incident beam power for the quenching, let us assume again that the initial conditions (T_0,Φ_0) are located on the coexistence curve. Then, by taking into account the expression of the coexistence curve $|\Phi_m-\Phi_M| = (\Delta\Phi)_0|1-T/T_C|^\beta$ [where $\beta=0.325$ for Ising $(d=3,\ n=1)$ fluids], the thermal quench depth $|\Phi_T^{\bar{q}=0}(x)/(\Phi_m-\Phi_M)|$, close to the center of the interference pattern, is given by [19]

$$\left|\frac{\Phi_T^{\bar{q}=0}(x)}{\Phi_M-\Phi_m}\right| = \frac{1}{2}\left[1-\left(1-\frac{T_E^{\bar{q}=0}(x)}{T_0+T_E^{\bar{q}=0}(x)-T_C}\right)^\beta\right] \approx \frac{\beta}{2}\frac{T_E^{\bar{q}=0}(x)}{(T_0-T_C)} \tag{23}$$

for weak thermal quenches $(T_E^{\bar{q}=0}(x)\ll T_0-T_C)$. To illustrate this supersaturation in Fig. 6, we have arbitrarily taken Φ_0 on the right-hand half of the coexistence curve (i.e., $\Phi_0>\Phi_C$). In fact, experimentally Φ_0 has to be chosen on the half which provides a refractive index of the droplets (i.e., of the phase Φ_m) larger than that of the surrounding phase (i.e., of the phase Φ_M) in order to ensure their optical trapping in illuminated areas.

To get the resulting droplet growth rate, note that conceptually this thermally driven quench is totally analogous to that obtained for a thermodiffusive process, since in the latter case the variation in composition is proportional to the overheating induced by the pumps; both processes have the same origin. Thus the growth is nonlocal and its rate is simply obtained by replacing $\Phi_{\rm th}^{\bar{q}=0}(x)$ by $\Phi_T^{\bar{q}=0}(x)$ in Eq. (13). We get

$$\frac{dR}{dt} = \frac{D^-}{R}\left(\frac{R}{\zeta_E}\right)\frac{K_1(R/\zeta_E)}{K_0(R/\zeta_E)} \times\left\{\left|\frac{(\Phi_T^{\bar{q}=0})_0}{\Phi_m-\Phi_M}\right|\frac{1}{\ln(\gamma a_{\rm cl}^2/a_0^2)}\left[-E_1\left(\frac{R^2}{a_0^2}\right)-\ln\left(\frac{R^2}{a_{\rm cl}^2}\right) +2\left(\frac{\zeta_E}{R}\right)\frac{K_0(R/\zeta_E)}{K_1(R/\zeta_E)}\left(\exp\left(-\frac{R^2}{a_0^2}\right)-1\right)\right]-\frac{d_0}{R}\right\}, \tag{24}$$

where

$$(\Phi_T^{\bar{q}=0})_0=\Phi_T^{\bar{q}=0}(x=0)=\frac{\beta}{2}\frac{\alpha_a P}{4\pi\Lambda_{\rm th}}\ln\left(\gamma\frac{a_{\rm cl}^2}{a_0^2}\right)\frac{1}{T_0-T_C}$$

is the optical quench in temperature on the axis of the interference pattern. As a consequence, the properties of the droplet growth rate and droplet growth law are in scaled units identical for thermal and thermodiffusive quenches. Figures 4 and 5 depict the expected behaviors if $(\Phi_{\rm th})_0$ is replaced by $(\Phi_T)_0$; the droplet grating reflectivity is also similar.

III. CHOSEN MEDIA

To experimentally investigate holographic grating formation resulting from laser-driven phase separation, we choose micellar phases of microemulsion as test media. We use quaternary components mixtures of water, oil, surfactant (soap), and cosurfactant (alcohol). Owing to the supramolecular size of the micelles and their in time organization, both electrostrictive and thermodiffusive processes can lead to sizable concentration variations in low power beams [15,27]. Moreover, the absorption of those mixtures in the visible wavelength window is often weak, leading to a small field-generated overheating. Thermal secondary effects, like bulk convection, thermocapillarity, or photophoresis, are thus negligible and do not disturb the diffusive nature of the composition variations induced by the wave. On the other hand, those mixtures feature critical behaviors; and close to a liquid–liquid critical point, microemulsions generally belong to the universality class $(d=3,\ n=1)$ of the Ising model. As a consequence, such media are particularly interesting to investigate droplet grating formations generated by laser-induced phase separation because (i) criticality enhances field couplings and (ii) the correlation length of density fluctuations inside the coexistence curve ξ^- is intrinsically large and diverges close to a critical point (i.e., $\xi^-=\xi_0^-|(T_0-T_C)/T_C|^{-\nu}$ with $\nu=0.63$). Two different mix-

TABLE I. Data used for evaluations of the different optical processes in the two mixtures tested in experiments; $(\partial\sqrt{\varepsilon_M}/\partial\Phi)_T$ is estimated from the Clausius-Mossotti relation and K_T^0 takes into account the first-order correction in Φ_0 of the viriel expansion.

Quaternary component mixture		Water/dodecane/ pentanol/SDS	Water/toluene/ butanol/SDS
ϱ_0	(kg/m^3)	780	870
ϱ_S	(kg/m^3)	983	983
$\Phi_{\text{sample}}(T_0<T_C)$		11%	13%
ξ_0^-	(nm)	1.1	2.0
η	(Pa.s)	$3.41\ 10^{-3}$	$1.93\ 10^{-3}$
Λ_{th}	(W/cm/K)	$1.45\ 10^{-3}$	$1.28\ 10^{-3}$
α_a	(m^{-1})	$5.58\ 10^{-2}$	$1.92\ 10^{-2}$
$\sqrt{\varepsilon_M}$		1.41	1.48
$(\partial\sqrt{\varepsilon_M}/\partial\Phi)_T$		$-2.62\ 10^{-2}$	$-1.25\ 10^{-1}$
k_T^0		3.0	0.4
K_T^0	(m^3/J)	$3.08\ 10^{-4}$	$1.77\ 10^{-3}$
$(\Delta\Phi)_0$		1.47	1.60

tures are used for the experimental investigation; their characteristics [15,22] are listed in Table I.

A. Nonlocal thermodiffusive phase transitions

To analyze phase transitions induced by a nonlocal coupling, here thermodiffusion, the selected system has the following mass composition: ultra pure water 5%, *n*-dodecane 78% and *n*-pentanol 12.2% of spectroscopic quality, and crystallized sodium dodecyl sulfate 4.8%. Located in the oil-rich part of the phase diagram [32], it features a water-in-oil micellar phase at room temperature which can be considered from the optical point of view as a set of nanometric dielectric spheres ($\approx$20 Å in radius at $T_0=20\,^\circ$C) suspended in an oil continuum. The chosen composition features a low critical temperature $T_C=32\,^\circ$C above, which the mixture phase-separates into two micellar phases of different micellar concentration; Fig. 1 is a schematic of the phase diagram of this mixture.

In this particular system, we have previously shown that electrostriction is negligible [16] because the optical polarizability of the micelles is extremely small due to the weak refractive index contrast between micelles and the surrounding oil (*n*-dodecane). The interaction between the wave and the micellar phase is mainly controlled by thermodiffusion: $\Phi_E(q,t)\approx\Phi_{\text{th}}(q,t)$. Since k_T is positive, thermodiffusion results in a local decrease of the micellar concentration inside the high field-intensity regions (i.e., $\Phi_{\text{th}}(q,t)<0$). Moreover, owing to the diverging behavior of the Soret constant k_T (i.e., $k_T=k_T^0[(T_0-T_C)/T_C]^{-\nu}$ with $\nu=0.63$) in the vicinity of the critical point, large k_T values can be achieved. Therefore, despite the very small optical absorption, $\alpha_a=5.5810^{-4}$ cm^{-1} at $\lambda_0=514$ mm, sizable concentration variations can be observed.

As depicted in Fig. 1, all the injected beam power is used for the quench in composition for $T_0>T_C$. This optical quenching results in the nucleation of droplets constituted by the minority phase Φ_m. Moreover, since the refractive index of the micelles is slightly smaller than that of the oil, the refractive index of Φ_m, and thus of the droplets, is larger than that of the surrounding majority phase Φ_M. As a consequence, these nucleated domains are drawn transversally in the high intensity regions by the electrostrictive forces and grow in the quenched area.

To give an order of magnitude of the different couplings involved in this mixture, let us consider a set of experiments described below. At $T_0-T_C=0.8$ K, for a total beam power $P=1.2$ W (i.e., 600 mW per pump beam), a beam waist $a_0=32\,\mu$m and a fringe spacing $\Lambda_0=3.5\,\mu$m, one finds the following stationary quench depths at the center of the interference pattern: $\Phi_{\text{th}}^{q=0}(x=0,t=\infty)/(\Phi_m-\Phi_M)=0.24$ corresponding to a temperature increase $T_E^{q=0}(x=0)=0.19$ K, and $\Phi_{\text{th}}^{q=q_0}(x=0,t=\infty)/(\Phi_m-\Phi_M)=6.10^{-5}$ corresponding to $T_E^{q=q_0}(x=0)=4.10^{-5}$ K. On the other hand, the electrostrictive and the thermal quench contributions are, respectively, $\Phi_{\text{el}}(x=0,t=\infty)/(\Phi_m-\Phi_M)=3.10^{-3}$ and $\Phi_T^{q=0}(x=0)/(\Phi_m-\Phi_M)=3.10^{-2}$. As expected, these evaluations show that the phase transition is almost completely driven by thermodiffusion (electrostrictive and heating contributions are at least ten time smaller), and thus by the Gaussian shape of the pump waves (the fringe contribution is totally negligible).

B. Local electrostrictive phase transitions

To investigate phase transitions induced by a local coupling, here electrostriction, the selected system has the following mass composition: ultra pure water 8.5%, toluene 71.4% and *n*-butanol 16.2% of spectroscopic quality, and crystallized sodium dodecyl sulfate 3.9%. Also located in the oil-rich part of the phase diagram [33], it also features a water-in-oil micellar phase at room temperature ($\approx$40 Å in micelle radius at $T_0=20\,^\circ$C). The chosen composition features a low critical temperature $T_C=31\,^\circ$C above which the mixture phase-separates into two micellar phases of different micellar concentration; its phase diagram is analogous to the $T_0>T_C$ part of that presented in Fig. 1.

In this system, it has been previously shown that electrostriction and thermodiffusion are both efficient [33]. However, as stated above, the characteristic time scale associated to concentration variations driven by a Fourier mode q is given by $\tau=1/(D^-q^2)$. Then, since $q\approx1/a_0$ for thermodiffusion [see Eq. (7b)] and $q=q_0=2\pi/\Lambda_0$ for electrostriction [see Eq. (8)], the phase transition is, in fact, completely driven by electrostriction on the fringes. For a ratio $q_0a_0\geqslant10$, the time scale for the electrostrictive variation in composition is one hundred times smaller than that driven by thermodiffusion. Due to this huge difference, we can assume that electrostriction drives totally the transition because finite size effects induced by the fringes on droplet growth also appear well before thermodiffusion is able to quench the mixture. Then $\Phi_E(q,t)\approx\Phi_{\text{el}}(q,t)$. Since $(\partial\sqrt{\varepsilon_M}/\partial\Phi)_T<0$ electrostriction also results in a local decrease in micellar concentration inside the high field-intensity regions (i.e., $\Phi_{\text{el}}(q,t)<0$). Moreover, owing to the diverging behavior of

the osmotic compressibility K_T (i.e., $K_T = K_T^0[(T_0 - T_C)/T_C]^{-\gamma}$ with $\gamma = 1.24$) in the vicinity of the critical point, large K_T values can be achieved and sizable concentration variations are observed at low beam powers.

As in the ''thermodiffusive microemulsion,'' for $T_0 > T_C$, all the injected beam power is used for the quench in composition and this dipolar quenching results in the nucleation of droplets constituted by the minority phase Φ_m. Moreover, the nucleated domains are automatically trapped transversally in the high intensity regions by the electrostrictive forces and grow in the illuminated area.

An order of magnitude of the different couplings involved in this mixture can also be estimated using the experimental conditions of a second set of experiments analyzed below. At $T_0 - T_C = 0.5\,\mathrm{K}$, for a total beam power $P = 600\,\mathrm{mW}$ (i.e., 300 mW per pump beam), a beam waist $a_0 = 23\,\mu\mathrm{m}$, and a fringe spacing $\Lambda_0 = 3.5\,\mu\mathrm{m}$, one finds the following stationary quench depth at the center of the interference pattern: $\Phi_{\mathrm{el}}(x=0,t=\infty)/(\Phi_m - \Phi_M) = 0.26$ which corresponds to the sum of the excitation by the $\overline{q}=0$ and $q=q_0$ modes, each mode contributing to one half of the supersaturation [remember that $I(q) \propto 2\delta(q) + \delta(q+q_0) + \delta(q-q_0)$ for plane waves]. Thus the electrostrictive supersaturation associated to the $q=q_0$ mode is $\Phi_{\mathrm{el}}^{q=q_0}(x=0,t=\infty)/(\Phi_m - \Phi_M) = 0.13$. Moreover, the thermodiffusive contributions are $\Phi_{\mathrm{th}}^{\overline{q}=0}(x=0,t=\infty)/(\Phi_m - \Phi_M) = 0.01$ corresponding to a temperature increase $T_E^{\overline{q}=0}(x=0) = 4.10^{-2}\,\mathrm{K}$ and $\Phi_{\mathrm{th}}^{q=q_0}(x=0,t=\infty)/(\Phi_m - \Phi_M) = 6.10^{-6}$ corresponding to $T_E^{q=q_0}(x=0) = 2.10^{-5}\,\mathrm{K}$. Finally, the amplitude of the supersaturation induced by the laser heating is $\Phi_T^{\overline{q}=0}(x=0)/(\Phi_m - \Phi_M) = 0.01$. We can conclude that the phase transition is almost completely driven by electrostriction in this second micellar phase of microemulsion. Moreover, for a dipolar coupling, the diffusion time scales of the $\overline{q}=0$ and $q=q_0$ modes [34] are, respectively, given by $a_0^2/4D^- = 130\,\mathrm{s}$ and $1/D^- q_0^2 = 0.3\,\mathrm{s}$. This important difference resulting from the associated diffusion length scales, respectively, a_0 and Λ_0, clearly illustrates the fact that the fringe contribution $q=q_0$ will trig much faster the phase transition than the $\overline{q}=0$ mode, even if stationary amplitudes of supersaturations are identical for both modes. As a consequence, R_{MAX}^E induced by the intensity modulation is reached well before the time scale $a_0^2/4\mathrm{D}^-$, and we can assume that the induced phase transition is completely dominated by the fringes.

IV. EXPERIMENTAL SETUP AND PROCEDURE

To analyze the reflectivity of the resulting droplet gratings, we use a four-wave mixing experiment, in which the phase transition is induced by two interfering pump beams and probed in Bragg conditions by a third beam at the same optical wavelength. The experimental setup is presented in Fig. 7. The liquid mixture is contained in a fused quartz cell (1 cm wide, 2 mm thick) thermally controlled by a water circulation regulated at better than 0.05 K. To generate the fringe pattern, the linear polarization of a c.w. TEM_{00} Ar^+ laser wave is adjusted by a λ/2 plate to be split into two

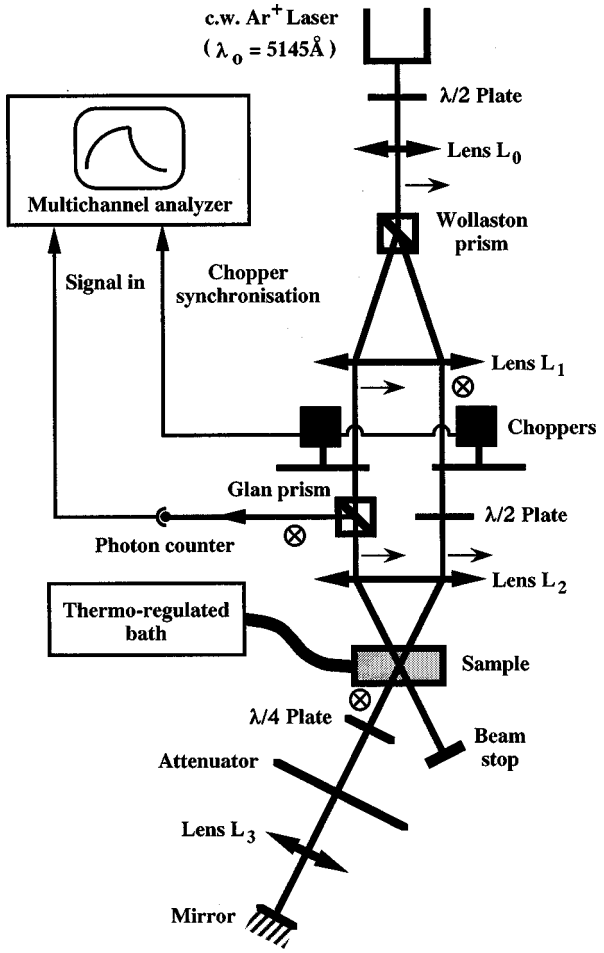

FIG. 7. Experimental setup. ↑ and ⊗ mimic the beam polarizations.

perpendicularly polarized beams of same intensity (the pump beams) by a Wollaston prism. An afocal system, composed of two lenses L_1 and L_2, recombines the pump beams in the cell with a definite angle θ and focuses these two beams at their intersection by imaging the beam waist generated by the lens L_0 on the Wollaston prism. θ and the beam waist a_0 at beam intersection can, respectively, be adjusted by changing the set (L_1, L_2) and L_0. A second λ/2 plate is placed on one beam to obtain pump waves of same polarization and make them interfere in the cell; the polarization is chosen so as to be in the x direction to induce repulsive dipole–dipole interactions between droplets trapped on the same fringe and to prevent as much as possible droplet coalescence. The fringe spacing is given by $\Lambda_0 = 2\pi/q_0 = \lambda_0/[2\sqrt{\varepsilon_M}\sin(\theta/2)]$, where $\lambda_0 = 514\,\mathrm{nm}$ is the optical wavelength in vacuum. The ratio between the pump beam diameters and the fringe spacing is always chosen to be larger than ten to obtain an efficient grating reflectivity and to fulfill the plane wave approximation used for the determination of this reflectivity. After propagation in the cell, one of the two pump beams is attenuated and retroreflected back through the sample by a mirror to play the role of the probe wave. The lens L_3 focuses the attenuated pump wave on the mirror to yield a probe beam extension in the cell identical to that of

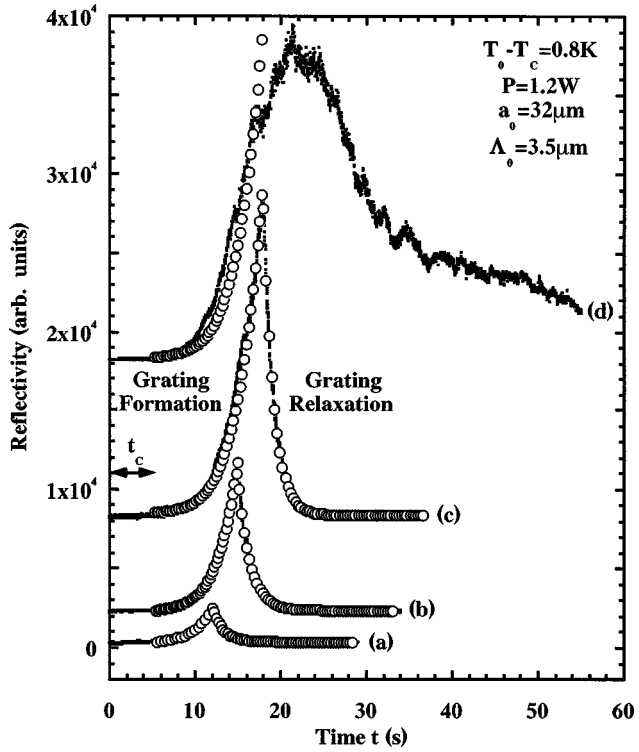

FIG. 8. Reflectivity of the probe beam induced by the formation and the relaxation of a thermodiffusive droplet grating when relaxation occurs at (a) $t_1=12$ s, (b) $t_1=15$ s, (c) $t_1=18$ s, and (d) $t_1=60$ s. The fits (empty circles) are performed according to Eqs. (20) and (22).

the pump waves. The probe beam polarization is rotated by an angle of 90° by means of the double travel through a λ/4 plate. Then, the wave reflected by the droplet grating has a polarization perpendicular to that of the pumps and can easily be extracted with a Glan prism. It is detected by means of a photon counter and accumulated with a multichannel analyzer.

A three-step experimental procedure is implemented to observe the grating formation induced by the transition. (i) At $t=0$, the two pump beams start to quench simultaneously the mixture. At $t=t_C$, droplets of the minority phase Φ_m are nucleated and trapped on the intensity maxima of the fringe pattern. A droplet grating is then generated. The grating formation and the domain growth make the reflectivity to increase. We deduce the mean droplet radius behavior $R(t)$ by fitting the reflectivity with Eqs. (20a)–(20c) and adjusting the nucleation time and the corresponding quench depth in the center of the interference pattern. In fact, to increase the accuracy of the measurements, several reflectivities, obtained for different increasing illumination times t_1, are used for the fitting procedure. (i) At $t=t_1$, the pump wave that is also not used as a probe wave, is stopped by a chopper, and the droplet grating relaxes. The decrease in reflectivity described by Eq. (21) allows a measurement of $R(t_1)$. (ii) At $t=t_2$, the second pump wave is stopped by a second chopper until a time t_3 (typically $t_3-t_2\approx 5t_1$) to ensure a thermodynamic relaxation of the system before starting a new accumulation on the multichannel analyzer.

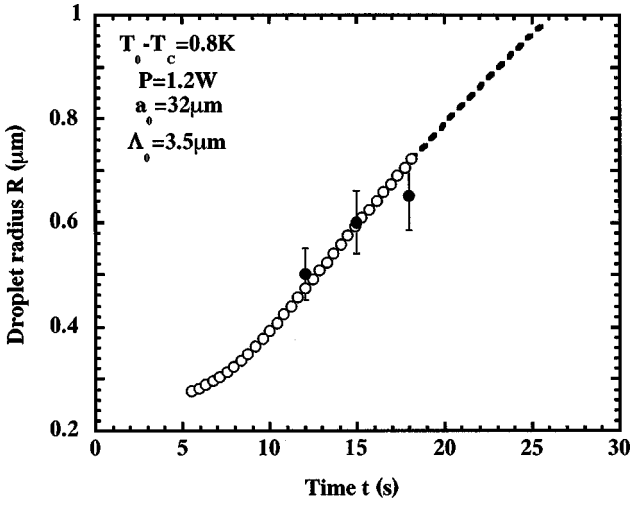

FIG. 9. Droplet growth law (empty circles) deduced from the fit of the grating formations of Fig. 8. The filled circles are the radii at t_1 deduced from the grating relaxations. The dashed line shows the continuation of the growth which was not measured.

V. EXPERIMENTAL RESULTS

A. Reflectivity induced by a nonlocal phase transition

To illustrate the above procedure, a typical experiment where the phase transition is dominated by a thermodiffusive process is presented in Fig. 8. The experiment is performed for four different illumination durations in the same conditions ($P=1.2$ W, $a_0=32$ μm, $\Lambda_0=3.5\,\mu$m, and $T_0-T_C=0.8$ K). From the three first grating relaxations we deduce the mean droplet radii at t_1. We find $R(t_1=12\ \text{s})=0.50$ μm, $R(t_1=15\ \text{s})=0.60$ μm and $R(t_1=18\ \text{s})=0.65$ μm. Besides, the grating formation of those three runs are fitted together with the same parameters. We obtain $t_C=5.5\pm0.3$ s and a mean initial supersaturation $\Phi_E(x=0,t=t_C)/(\Phi_m-\Phi_M)=0.026\pm0.003$, which corresponds to a mean critical radius $R_C=0.26\pm0.03\,\mu$m; errors are $dR/R\approx dR_C/R_C\leqslant 10\%$, $dt_C/t_C\leqslant 5\%$, and $d\Phi_E/\Phi_E\leqslant 10\%$ [28]. The resulting droplet growth $R(t)$ is represented in Fig. 9. Figure 9 also shows that the droplet radii measured from the grating relaxations are in good agreement with the growth law deduced independently from grating formations.

On the other hand, Fig. 8 illustrates the behavior of the reflectivity for an illumination time $t_1=60$ s. After reaching a maximum, the amplitude of the reflectivity starts decreasing continuously from $t\approx 22$ s. According to Fig. 9, this corresponds to a mean droplet radius of 0.9 μm, close to $\Lambda_0/4$ for which the efficiency of the induced grating is the largest. Then, as expected for a grating driven by thermodiffusion, the droplet growth does not saturate in presence of fringes. Finally, we can observe that the measured value of $\Phi_E(x=0,t=t_C)/(\Phi_m-\Phi_M)$ needed to initiate nucleation is much smaller than the final thermodiffusive supersaturation $\Phi_{\text{th}}^{\bar{q}=0}(x=0,t=\infty)/(\Phi_m-\Phi_M)=0.24$. This proves that the phase separation is induced before the steady state quench in concentration is reached, as it could be expected. Since the characteristic time scale of a thermodiffusive quench in com-

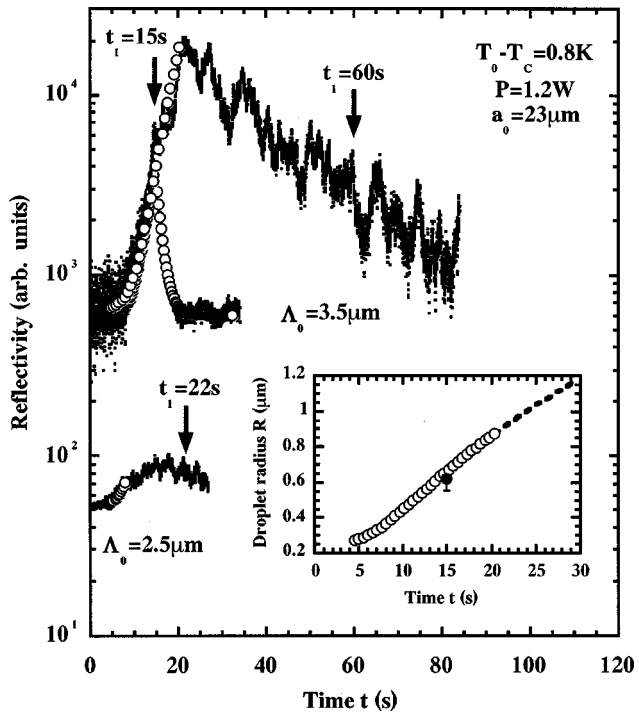

FIG. 10. Reflectivity of the probe beam induced by the formation and the relaxation of a thermodiffusive droplet grating for different fringe spacings. For $\Lambda_0=3.5\,\mu$m (respectively $\Lambda_0=2.5\,\mu$m) relaxation occurs at $t_1=15$ s and $t_1=60$ s (respectively $t_1=22$ s). The fits (empty circles) are performed according to Eqs. (20) and (22). Inset: droplet growth law (empty circles) deduced from the grating formation for $\Lambda_0=3.5\,\mu$m and $t_1=15$ s. The filled circle is the radius deduced from the grating relaxation at $t_1=15$ s and the dashed line shows the continuation of the growth which was not measured.

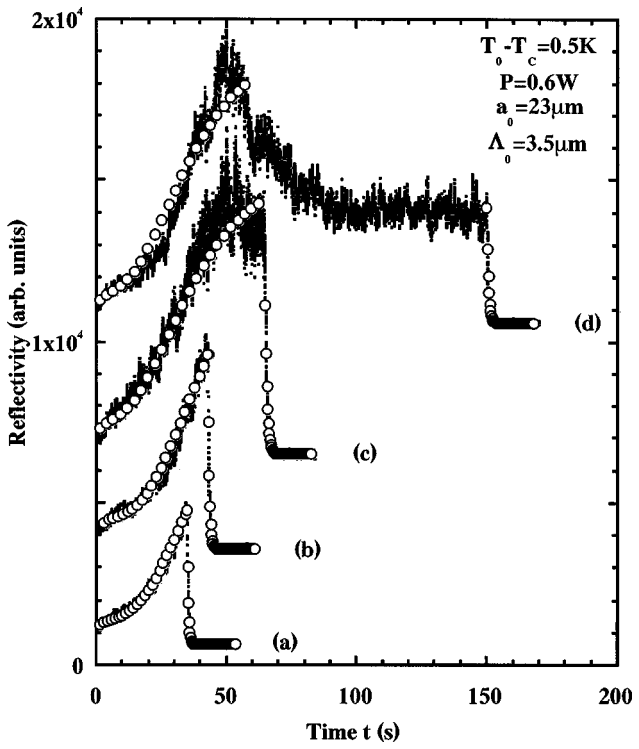

FIG. 11. Reflectivity of the probe beam induced by the formation and the relaxation of an electrostrictive droplet grating when relaxation occurs at (a) $t_1=35$ s, (b) $t_1=45$ s, (c) $t_1=65$ s, and (d) $t_1=150$ s. The fits (empty circles) are performed according to Eqs. (20) and (22).

position is given by a_0^2/D^- [34], we also conclude that if nucleation was homogeneous, the time needed to reach $\Phi_{\rm th}^{q=0}(x=0,t=t_C)/(\Phi_m-\Phi_M)=0.026$ measured in the experiment would be of the order of 75 s. As already demonstrated by a different reasoning [28], this numerical application illustrates again that nucleation is essentially heterogeneous in mixtures, and explains why the fit of the grating formations are in agreement with the hypothesis that a majority of droplets are nucleated at the same mean time t_C. The unavoidable seeds present in the bulk decrease the nucleation barrier and thus accelerate the decay of a metastable state compared to a homogeneous nucleation picture.

According to Eqs. (7a) and (7b), two optical parameters can be varied to analyze the influence of the dynamics of the quench in concentration on grating formation: the total power P injected in the medium and the beam waist a_0 of the pump waves at intersection. The behaviors in P and a_0 have already been described when analyzing the early stage kinetics of the induced transition [34]. However, even if Λ_0 is not pertinent for a nonlocal quench, it strongly influences the largest observable reflectivity. To illustrate this aspect, Fig. 10 shows two experiments realized in the same conditions as those used in Figs. 8 and 9 but for another beam waist ($a_0=23\,\mu$m) and for two different fringe spacings, $\Lambda_0=2.5\,\mu$m and $\Lambda_0=3.5\,\mu$m. To obtain the droplet growth law for $a_0=23\,\mu$m, a first run at $\Lambda_0=3.5\,\mu$m investigates the droplet grating before saturation at $t_1=15$ s. From the grating formation we get $t_C=4.5\pm0.2$ s and a mean initial supersaturation $\Phi_E(x=0,t=t_C)/(\Phi_m-\Phi_M)=0.029\pm0.003$ which corresponds to a mean critical radius $R_C=0.27\pm0.03\,\mu$m; from the relaxation, we find $R(t_1=15\,\text{s})=0.62\,\mu$m. Then the experiment is realized twice above saturation for $\Lambda_0=3.5\,\mu$m and $\Lambda_0=2.5\,\mu$m; the chosen illumination times are, respectively, $t_1=60$ s and $t_1=22$ s. For $\Lambda_0=3.5\,\mu$m (resp. $\Lambda_0=2.5\,\mu$m) the reflectivity reaches a maximum at $t\approx20$ s (resp. $t\approx15$ s) which, according to the inset of Fig. 10, corresponds to a mean droplet radius of the order of 0.9 μm (resp. 0.65 μm), close to $\Lambda_0/4$. Then, the reflectivity decreases continuously.

As a consequence, when driven by a nonlocal process, the temporal behavior of the reflectivity is characterized by a sharp slope, as long as the size of the growing droplet is small compared to the fringe spacing. Then, the slope reaches a maximum ($R(t)\approx\Lambda_0/4$), reverses irreversibly ($R(t)>\Lambda_0/4$), and the reflectivity vanishes because droplet size larger than Λ_0 are allowed by the kinetics of the induced phase transition, but evidently blur the periodicity of the induced structure.

B. Reflectivity induced by a local phase transition

Using the same experimental procedure as that described above, a typical experiment where the phase transition is

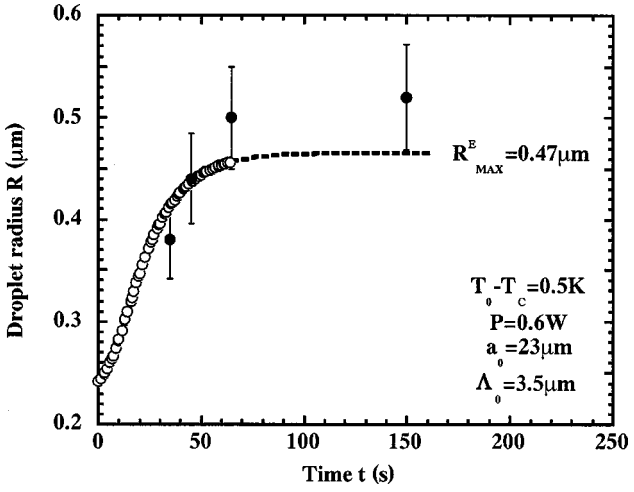

FIG. 12. Droplet growth law (empty circles) deduced from the fit of the grating formations of Fig. 11. The filled circles are the radii at t_1 deduced from the grating relaxations. The dashed line shows the continuation of the growth which was not measured from the grating formation.

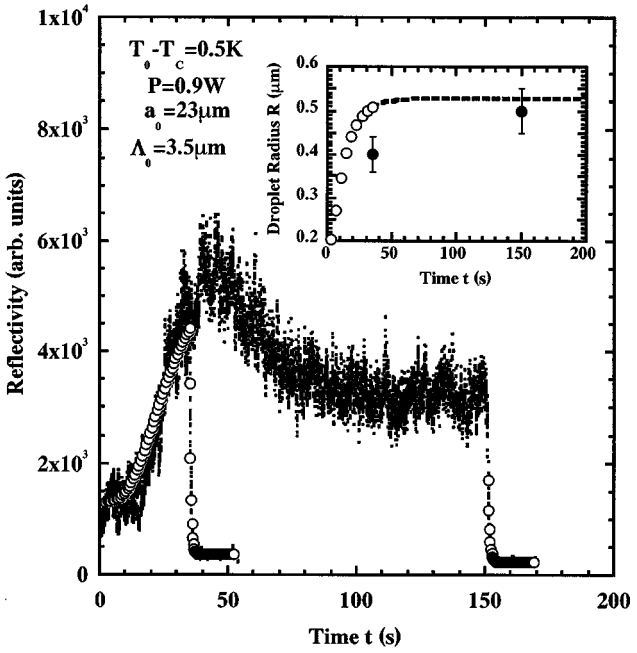

FIG. 13. Reflectivity of the probe beam induced by the formation and the relaxation of an electrostrictive droplet grating when relaxation occurs at (a) $t_1=35$ s and (b) $t_1=150$ s. The fits (empty circles) are performed according to Eqs. (20) and (22); the grating formation leads to $t_C\approx 0.5$ s and a mean initial supersaturation $\Phi_E(x=0,t=t_C)/(\Phi_m-\Phi_M)=0.12\pm 0.01$ which corresponds to a mean critical radius $R_C=0.19\pm 0.02\ \mu$m. Inset: droplet growth law (empty circles) deduced from the grating formation when $t_1=35$ s. The filled circles are the radii deduced from the grating relaxations [$R(t_1=35\text{ s})=0.39\ \mu$m, $R(t_1=150\text{ s})=0.50\ \mu$m] and the dashed line shows the continuation of the growth which was not measured from the grating formation. Note that $R(t_1=150\text{ s})$ is close to the expected saturation $R^E_{\mathrm{MAX}}=0.53\ \mu$m.

dominated by an electrostrictive process is presented in Fig. 11. The experiment is performed for four different illumination durations in the same conditions ($P=0.6$ W, $a_0=23\ \mu$m, $\Lambda_0=3.5\ \mu$m and $T_0-T_C=0.5$ K). From the grating relaxations we deduce the mean droplet radii for those four values of t_1. We find $R(t=35\text{ s})=0.38\ \mu$m, $R(t_1=45\text{ s})=0.44\ \mu$m, $R(t_1=65\text{ s})=0.50\ \mu$m, and $R(t_1=150\text{ s})=0.52\ \mu$m. Besides, the grating formation of those four runs are fitted together with the same parameters. We obtain $t_C\approx 0.5$ s and a mean initial supersaturation $\Phi_E(x=0,t=t_C)/(\Phi_m-\Phi_M)=0.10\pm 0.01$, which corresponds to a mean critical radius $R_C=0.23\pm 0.02\ \mu$m. As expected, the small value of t_C shows that the phase transition is totally driven by the characteristic time scale of mass diffusion on the fringes $1/D^- q_0^2=0.3$ s. The resulting droplet growth $R(t)$ and the set of droplet radii measured from the grating relaxations are represented in Fig. 12; a good agreement is observed.

On the other hand, the expected saturation calculated from Eq. (11) is $R^E_{\mathrm{MAX}}=0.47\ \mu$m, close to the saturation observed experimentally at $t_1=65$ s and $t_1=150$ s. Then, despite the decrease in efficiency (due to an increase in scattering of the pumps, induced by the droplet growth, and thus to a decrease in intensity of the probe in our experimental setup) observed for $t_1=150$ s, this experiment clearly shows that droplet growth driven by electrostriction is totally monitored by the fringes. The reflectivity reaches a stationary value linked to the saturation of the droplet growth to R^E_{MAX}. This behavior, also illustrated in Fig. 13 for a different injected beam power, contrasts with that observed in presence of a nonlocal coupling, and allows a clear distinction between both processes. Finally, we can observe that the measured value of $\Phi_E(x=0,t=t_C)/(\Phi_m-\Phi_M)$ needed to initiate nucleation is in agreement with the calculated final electrostrictive supersaturation induced by the fringes $\Phi_{\mathrm{el}}^{\overline{q=0}}(x=0,t=\infty)/(\Phi_m-\Phi_M)=0.13$. This point confirms the local character of electrostriction; the smallness of the characteristic time scale of diffusion on the fringes leads to the fact that the quench in composition is almost stationary before the phase separation occurs.

We have also analyzed the beam power influence on the grating formation for three different beam powers: $P=0.45$, 0.9, and 1.2 W. The experiment is illustrated in Fig. 14. Saturation of the reflectivity appears respectively at $t_{\mathrm{MAX}}=55$, 32, and 27 s. As expected, the duration of the droplet growth decreases for increasing beam powers. According to the model, a first-order development in $R-R^E_{\mathrm{MAX}}$ of the electrostrictive droplet growth rate equation shows that the characteristic time scale t_{MAX} needed to reach R^E_{MAX} behaves as $(\Phi_m-\Phi_M)/\Phi_E(x=0,t=t_C)$ for deep quenches. At constant beam-waist, this means that $t_{\mathrm{MAX}}\propto 1/P$ for an electrostrictive coupling. As illustrated in the inset of Fig. 14, we recover the expected behavior, but with a slightly different power law ($t_{\mathrm{MAX}}\propto P^{-0.74}$ is measured instead of $t_{\mathrm{MAX}}\propto P^{-1}$). The discrepancy could be explained by the fact that the induced supersaturations are not sufficiently deep to totally eliminate the dependence of R^E_{MAX} on the quench depth.

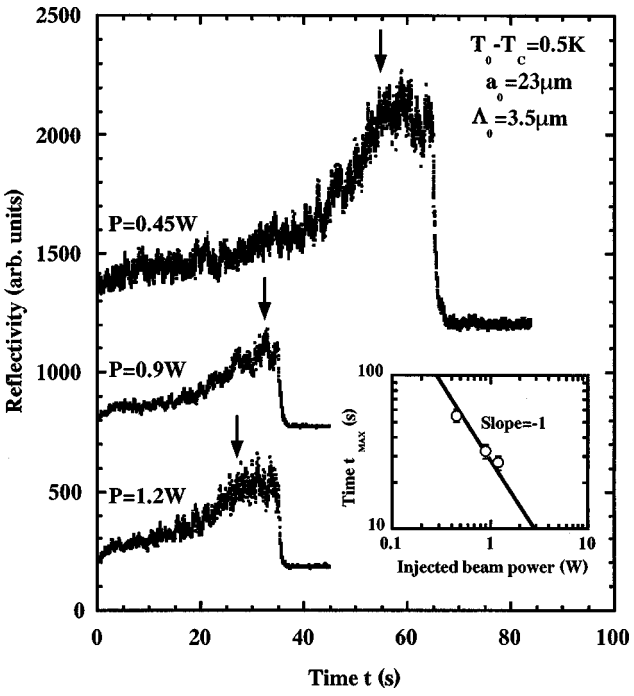

FIG. 14. Reflectivity of the probe beam induced by the formation and the relaxation of an electrostrictive droplet grating for different injected beam powers. Arrows indicate the beginning of the saturation of the reflectivities. Inset: variation of the time t_{MAX} needed for saturation of the reflectivity as a function of the injected beam power.

VI. CONCLUSION

In the present paper, we have investigated the kinetics of holographic grating formation resulting from laser-induced phase separation. This study was undertaken in view of understanding the influence of locality (or nonlocality) of the excitation process on the formation of bulk holographic gratings, and also because of its important technologic significance in material science, particularly in patterning diffracting elements. Preliminary results needed a theoretical background in order to understand the different observations and to investigate the potentialities of the processes involved. To achieve this goal, we used interfering c.w. laser waves to quench binary liquid mixtures and to optically trap the nucleated domains in the high intensity regions. Essentially, three different couplings can induce transition: electrostriction, thermodiffusion, and laser heating. As photopolymerization, electrostriction belongs to the family of local processes. This means that the medium is excited by the Fourier components of the field distribution. On the other hand, as in the solvent evaporation technique, thermodiffusion and laser heating have a dissipative origin due to light absorption. Then, they do not follow exactly the electromagnetic field distribution and the resulting nonlocal response of the medium has an important contribution around the $q=0$ Fourier mode. As a consequence, the morphology of holographic grating generated by laser-induced phase transitions can be very different depending on the excitation process. To analyze the kinetics properties of the induced patterning, we started from the very beginning of the optical excitation process by describing theoretically the optical quenching mechanisms induced by two interfering pump beams, and we derived for each coupling the growth rate of the fringe trapped droplets nucleated during the induced phase transition. It clearly appears that the growth of droplets nucleated by a local coupling is completely monitored by the fringes, while nonlocal excitation leads to a growth controlled by the size of the pumps. To probe these behaviors, we have experimentally analyzed the real time formation of the resulting droplet grating for both local and nonlocal excitations. In presence of a local coupling, the reflectivity of the induced droplet grating reaches a stationary value due to the saturation of the droplet growth induced by the finite size of the fringe; the fringe spacing self-calibrates the final size of the droplets. On the other hand, since a nonlocal process is mainly sensitive to the shape of the pumps, droplet growth is, in this case, monitored by the beam-waist. Then, after reaching a maximum, the reflectivity of an induced droplet grating decreases continuously and vanishes when droplet diameters become larger than the fringe spacing. All the experiments are interpreted using our general model, and there is good quantitative agreement. As a consequence, even if we develop our investigation in simple binary liquid mixtures (which clearly cannot be considered as useful media in terms of applications) to increase the accuracy of the comparison between theory and experiments, it can easily be extended to other phase-separating mixtures because the behaviors associated to the locality or the nonlocality of the excitation are totally generic. For example, the kinetics of separation in polymer mixtures [35] and polymer dispersed liquid crystals [36] starts to be reasonably well understood, and optical quenching by a fringe pattern involving nonlocal couplings (resp. local excitations) like laser heating or laser-induced solvent evaporation (resp. laser-induced dipoles) can easily be treated from the thermodynamic point of view; laser heating is studied briefly in this paper and solvent evaporation (resp. laser-induced dipoles) behaves as thermodiffusion (resp. electrostriction). In fact, the main problem of such investigation is to be able to describe the kinetics of the induced transition in presence of the electromagnetic field, and our choice was motivated by the existence of such a theory in the Universality class ($d=1,\ n=3$) of the Ising model.

As a conclusion, the present work shows how the dynamics of holographic grating formation resulting from a laser-induced first order phase transition can be investigated, and explains the influence of the excitation mechanism on their performances. It may serve as a first step towards a better understanding of the origin of the resulting dynamic organization and to predict its evolution.

ACKNOWLEDGMENTS

We are grateful to Professor A. Ducasse for valuable discussions and his constant encouragement. We thank J. Plantard and M. Winckert for technical assistance. This work was partly supported by the Région Aquitaine.

[1] H. Nishihara, M. Haruna, and T. Suhara, *Optical Integrated Circuits* (McGraw-Hill, New York, 1985).
[2] P. Ayräs, J. T. Rantala, S. Honkanen, S. B. Mendes, and N. Peyghambarian, Opt. Commun. **162**, 215 (1999).
[3] M. G. Schnoes, L. Dhar, M. L. Schilling, S. S. Patel, and P. Wiltzius, Opt. Lett. **24**, 658 (1999).
[4] L. Dhar, K. Curtis, M. Tackitt, M. Schilling, S. Campbell, W. Wilson, A. Hill, C. Boyd, N. Levinos, and A. Harris, Opt. Lett. **23**, 1710 (1998).
[5] E. Soergel and W. Krieger, Phys. Rev. Lett. **83**, 2336 (1999).
[6] J. W. Doane, in *Liquid Crystals: Applications and Uses*, edited by B. Bahadur (World Scientific, Singapore, 1990).
[7] J. Y. Kim and P. Palffy-Muhoray, Mol. Cryst. Liq. Cryst. **203**, 93 (1991).
[8] A. Golemme, G. Arabia, and G. Chidichimo, Mol. Cryst. Liq. Cryst. Sci. Technol., Sect. A **243**, 185 (1994).
[9] J. Y. Kim, C. H. Cho, P. Palffy-Muhoray, M. Mustafa, and T. Kyu, Phys. Rev. Lett. **71**, 2232 (1993).
[10] D. W. Oxtoby, Acc. Chem. Res. **31**, 91 (1998).
[11] G. Eyring and M. D. Fayer, J. Appl. Phys. **55**, 4072 (1984).
[12] R. L. Sutherland, V. P. Tondiglia, L. V. Natarajan, T. J. Bunning, and W. W. Adams, Appl. Phys. Lett. **64**, 1074 (1994); T. J. Bunning, L. V. Natarajan, V. P. Tondiglia, R. L. Sutherland, D. L. Vezie, and W. W. Adams, Polymer **36**, 2699 (1995).
[13] G. Zhao and P. Mouroulis, J. Mod. Opt. **41**, 1929 (1994); S. Piazzolla and K. Jenkins, Opt. Lett. **21**, 1075 (1996); V. L. Colvin, R. G. Larson, A. L. Harris, and M. L. Schilling, J. Appl. Phys. **81**, 5913 (1997); J. H. Kwon, H. C. Hwang, and K. C. Woo, J. Opt. Soc. Am. B **16**, 1651 (1999); G. M. Karpov, V. V. Obukhovsky, T. N. Smirnova, and V. V. Lemeshko, Opt. Commun. **174**, 391 (2000); C. C. Bowley and G. P. Crawford, Appl. Phys. Lett. **76**, 2235 (2000).
[14] J. D. Gunton, M. San Miguel, and P. S. Sahni, in *Phase Transition and Critical Phenomena*, edited by C. Domb and J. L. Lebowitz (Academic, New York, 1983), Vol. 8.
[15] B. Jean-Jean, E. Freysz, A. Ponton, A. Ducasse, and B. Pouligny, Phys. Rev. A **39**, 5268 (1989); E. Freysz, E. Laffon, J. P. Delville, and A. Ducasse, Phys. Rev. E **49**, 2141 (1994).
[16] J. P. Delville, C. Lalaude, E. Freysz, and A. Ducasse, Phys. Rev. E **49**, 4145 (1994).
[17] A. J. Palmer, Opt. Lett. **5**, 54 (1980).
[18] M. Giglio and A. Vendramini, Phys. Rev. Lett. **34**, 561 (1975); **38**, 26 (1977).
[19] J. P. Delville, C. Lalaude, and A. Ducasse, Physica A **262**, 40 (1999).
[20] W. H. Lowdermilk and N. Bloembergen, Phys. Rev. A **5**, 1423 (1972).
[21] R. D. Mountain and J. M. Deutch, J. Chem. Phys. **50**, 1103 (1969).
[22] C. Lalaude, J. P. Delville, S. Buil, and A. Ducasse, Phys. Rev. Lett. **78**, 2156 (1997); J. P. Delville, C. Lalaude, S. Buil, and A. Ducasse, Phys. Rev. E **59**, 5804 (1999).
[23] S. Puri, K. Binder, and S. Dattagupta, Phys. Rev. B **46**, 98 (1992).
[24] J. A. Marqusee, J. Chem. Phys. **81**, 976 (1984).
[25] S. R. Corriel and R. L. Parker, J. Appl. Phys. **36**, 632 (1965).
[26] J. S. Langer and A. J. Schwartz, Phys. Rev. A **21**, 948 (1980).
[27] E. Freysz, E. Laffon, and A. Ducasse, Opt. Lett. **16**, 1644 (1991).
[28] S. Buil, J. P. Delville, E. Freysz, and A. Ducasse, Opt. Lett. **23**, 1334 (1998); S. Buil, J. P. Delville, and A. Ducasse, Phys. Rev. Lett. **82**, 1895 (1999).
[29] P. W. Smith, A. Ashkin, and W. J. Tomlinson, Opt. Lett. **6**, 284 (1981).
[30] E. D. Siebert and C. M. Knobler, Phys. Rev. Lett. **52**, 1133 (1984).
[31] J. Hofkens, J. Hotta, K. Sazaki, H. Masujara, and K. Iwai, Langmuir **13**, 414 (1997).
[32] D. Gazeau, E. Freysz, and A. M. Bellocq, Europhys. Lett. **9**, 833 (1989).
[33] B. Jean-Jean, E. Freysz, A. Ducasse, and B. Pouligny, Europhys. Lett. **8**, 219 (1988).
[34] S. Buil, J. P. Delville, and A. Ducasse, Eur. Phys. J. E **2**, 105 (2000).
[35] H. Takeno, E. Nakamura, and T. Hashimoto, J. Chem. Phys. **110**, 3612 (1999).
[36] J. B. Nephew, T. C. Nihei, and S. A. Carter, Phys. Rev. Lett. **80**, 3276 (1998); J. C. Lee, Phys. Rev. E **60**, 1930 (1999); H. W. Chin and T. Kyu, J. Chem. Phys. **110**, 5998 (1999).